Articles

Thermodynamics of Melittin Binding to Lipid Bilayers. Aggregation and Pore Formation†

Gabriela Klocek,‡ Therese Schulthess,‡ Yechiel Shai,§ and Joachim Seelig*,‡

Department of Biophysical Chemistry, Biozentrum, University of Basel, Klingelbergstrasse 50/70, CH-4056 Basel, Switzerland, and Department of Biological Chemistry, The Weizmann Institute of Science, Rehovot 76100, Israel

Received November 18, 2008; Revised Manuscript Received January 27, 2009

ABSTRACT: Lipid membranes act as catalysts for protein folding. Both α-helical and β-sheet structures can be induced by the interaction of peptides or proteins with lipid surfaces. Melittin, the main component of bee venom, is a particularly well-studied example for the membrane-induced random coil-to-α-helix transition. Melittin in water adopts essentially a random coil conformation. The cationic amphipathic molecule has a high affinity for neutral and anionic lipid membranes and exhibits ∼50−65% α-helix conformation in the membrane-bound state. At higher melittin concentrations, the peptide forms aggregates or pores in the membrane. In spite of the long-standing interest in melittin−lipid interactions, no systematic thermodynamic study is available. This is probably caused by the complexity of the binding process. Melittin binding to lipid vesicles is fast and occurs within milliseconds, but the binding process involves at least four steps, namely, (i) the electrostatic attraction of the cationic peptide to an anionic membrane surface, (ii) the hydrophobic insertion into the lipid membrane, (iii) the conformational change from random coil to α-helix, and (iv) peptide aggregation in the lipid phase. We have combined microelectrophoresis (measurement of the ζ potential), isothermal titration calorimetry, and circular dichroism spectroscopy to provide a thermodynamic analysis of the individual binding steps. We have compared melittin with a synthetic analogue, [D]-$V^{5,8}$,I^{17},K^{21}-melittin, for which α-helix formation is suppressed and replaced by β-structure formation. The comparison reveals that the thermodynamic parameters for the membrane-induced α-helix formation of melittin are identical to those observed earlier for other peptides with an enthalpy h_{helix} of −0.7 kcal/mol and a free energy g_{helix} of −0.2 kcal/mol per peptide residue. These thermodynamic parameters hence appear to be of general validity for lipid-induced membrane folding. As g_{helix} is negative, it further follows that helix formation leads to an enhanced membrane binding for the peptides or proteins involved. In this study, melittin binds by ∼2 orders of magnitude better to the lipid membrane than [D]-$V^{5,8}$,I^{17},K^{21}-melittin which cannot form an α-helix. We also found conditions under which the isothermal titration experiment reports only the aggregation process. Melittin aggregation is an entropy-driven process with an endothermic heat of reaction (ΔH_{agg}) of ∼2 kcal/mol and an aggregation constant of 20−40 M^{-1}.

Melittin is the major protein component of the venom of the honey bee *Apis melifera* and has hemolytic and antimicrobial properties (*1, 2*). It is probably the most prominent and most widely studied membrane-interacting peptide, and a large number of studies have been undertaken to elucidate the conformational properties and the action mechanism of melittin (*3*−*8*). Melittin in solution is mainly random coil but adopts an α-helical conformation when bound to sulfated cell surface sugars (*7*) or to lipid membranes (*8*). It is then surprising that no systematic thermodynamic study of the interaction of melittin with lipid membranes is available. A few binding constants and binding isotherms have been reported (*4, 8*−*13*), but no data are available on the binding enthalpy and entropy or on the temperature dependence of the thermodynamic parameters.

Melittin forms tetramers in aqueous solutions at sufficiently high concentrations (*14*−*16*). In lipid membranes, melittin also forms peptidic aggregates (*6*), but again no systematic thermodynamic data are available.

The binding of cationic melittin (z_p = 5−6) to anionic lipid vesicles is initiated by an electrostatic attraction to the membrane surface. The concentration of melittin near the plane of binding is considerably higher than in bulk solution. Electrostatic attraction is then followed by chemical adsorption where melittin inserts into the lipid bilayer and partially

† Supported by Swiss National Science Foundation Grant 3100-107793. Y.S. is the incumbent of the Harold S. and Harriet B. Brady Professional Chair in Cancer Research.

* To whom correspondence should be addressed. Telephone: +41-61-267 2190. Fax: +41-61-267 2189. E-mail: joachim.seelig@unibas.ch.

‡ University of Basel.

§ The Weizmann Institute of Science.

10.1021/bi802127h CCC: $40.75
Published on Web 01/27/2009

compensates for the electric charge of the membrane surface. Membrane insertion is accompanied by a change in the peptide conformation from mainly random coil in buffer to 50−65% α-helix when membrane-bound. Melittin is distributed evenly between the two half-layers of the lipid vesicle and, at a defined threshold concentration, starts to aggregate.

We have used ITC[1] to resolve the energetics of the individual binding steps. While the electrostatic attraction to the membrane surface does not involve any significant heat change, the ensuing processes of membrane insertion, helix formation, and peptide aggregation all contribute to the measured heat flow. Fortunately, the analysis of the ITC binding isotherms is simplified by two observations. First, by employing [D]-$V^{5,8}$,I^{17},K^{21}-melittin, where four L-amino acids are replaced with their D-enantiomers (*17*), the random coil-to-α-helix transition could be eliminated, and the calorimetric data reflect the melittin binding step. Second, we found calorimetric conditions where the aggregation of melittin in the membrane could be studied in a manner independent of other processes. This was possible because the endothermic heat of melittin binding and the exothermic heat of α-helix formation cancel each other accidentally at 28 °C. The observed heat changes at 28 °C can thus be assigned exclusively to the aggregation process.

In the following, we describe experiments on (i) the electrophoretic mobility (ζ potential) of lipid vesicles as a function of melittin concentration, (ii) the conformational changes of melittin and [D]-$V^{5,8}$,I^{17},K^{21}-melittin upon lipid binding using CD spectroscopy, and (iii) ITC-measured binding isotherms of melittin and [D]-$V^{5,8}$,I^{17},K^{21}-melittin. The membrane vesicles were of homogeneous size (∼100 nm) and were composed of 1-palmitoyl-2-oleoyl-*sn*-glycero-3-phosphocholine (POPC) and 1-palmitoyl-2-oleoyl-*sn*-glycero-3-phosphoglycerol (POPG) at a 3:1 molar ratio, mimicking the lipid composition of some bacterial membranes. We used chemically synthesized melittin as melittin from natural sources appears to produce artifacts. The electrophoretic and thermodynamic results were correlated with the changes in the melittin conformation and provided quantitative insights of general relevance into the problems of membrane-induced peptide folding and aggregation.

MATERIALS AND METHODS

Materials. Melittin was purchased from BACHEM AG (Bubendorf BL, Switzerland) (purity of >97% determined by reversed phase HPLC). [D]-$V^{5,8}$,I^{17},K^{21}-melittin was synthesized as described previously (*17*). The concentration of the peptides in the aqueous solution was determined by UV spectroscopy at 280 nm using an absorption coefficient of 5570 M^{-1} cm^{-1}. 1-Palmitoyl-2-oleoyl-*sn*-glycero-3-phosphatidylcholine (POPC) and 1-palmitoyl-2-oleoyl-*sn*-glycero-3-phosphatidylglycerol (POPG) were purchased from Avanti Polar Lipids Inc. (Alabaster, AL).

All other chemicals were analytical or reagent grade. Tris buffer [25 mM tris(hydroxyl)aminoethane and 50 mM NaCl (pH 7.4)] was prepared from 18 MΩ water obtained from a NANOpure A filtration system. The samples were degassed immediately before use.

Preparation of Lipid Vesicles. A defined amount of POPC was dried from a stock solution in chloroform under a gentle stream of nitrogen followed by a high vacuum overnight. The amount of POPC was weighed and mixed with a defined volume of POPG stock solution in chloroform to yield a POPC:POPG molar ratio of 3:1. The solvent was removed under a gentle stream of nitrogen, and the thin lipid film was exposed to high vacuum overnight and weighed again. The lipids were resuspended in buffer with gentle vortex mixing, leading to multilamellar vesicles (MLVs) with a final lipid concentration of 10−20 mM. Large unilamellar vesicles (LUVs) were prepared by extrusions of MLV suspensions using an extruder. After five consecutive freeze−thaw cycles, MLVs were extruded 12 times through a polycarbonate membrane with a pore diameter of 100 nm (Whatman, Clifton, NJ). Small unilamellar vesicles (SUVs) for the CD measurements were prepared by sonication of the lipid suspension using a titanium tip ultrasonicator (Branson Sonifier, Danbury, CT) until an almost clear solution was obtained (20 min). Metal debris from the sonicator tip was removed by centrifugation for 2 min in an Eppendorf 5415 C benchtop centrifuge (Vaudaux-Eppendorf AG, Schonenbuch, Switzerland).

Isothermal Titration Calorimetry. All measurements were taken with a MicroCal VP-ITC calorimeter (MicroCal, Northampton, MA). Lipid-into-peptide titrations were performed by injecting 10 μL aliquots of lipid suspension into the calorimeter cell (V_{cell} = 1.4037 mL) containing the peptide at a concentration of typically 19−25 μM, at constant time intervals of 10 min. Peptide-into-lipid titrations were performed by injecting 10 μL aliquots of the peptide solution at a concentration of typically 200−250 μM into the calorimeter cell containing the lipid suspension at a concentration of 10−20 mM.

The heats of dilution were determined in the control titrations by injecting the lipid solution or the peptide solution into pure buffer and were included in the final analysis.

Size and ζ Potential Measurements. The size and ζ potential of LUVs (total lipid concentration of 40 μM) were measured in a Zetasizer Nano ZS instrument (Malvern Instruments Ltd., Worcestershire, U.K.) in the presence of various peptide concentrations. Samples were prepared in Tris buffer [25 mM Tris and 50 mM NaCl (pH 7.4)], and measurements were taken at 30 °C.

Release of Calcein from Lipid Vesicles. Calcein release measurements were performed on a fluorescence spectrophotometer F-4500 instrument (Hitachi, Tokyo, Japan). A lipid film [POPC/POPG (3:1)] was prepared as described above, and 10 mM Tris buffer (pH 7.4) containing 50 mM calcein and 5 mM EDTA was added. After five freeze−thaw cycles, MLVs were extruded 12 times through a polycarbonate membrane with a pore diameter of 100 nm (Whatman, Clifton, NJ). Unentrapped calcein was removed from the large unilamellar vesicles (LUVs) by gel filtration on a Sephadex G75 column equilibrated with 10 mM Tris and 130 mM KCl (pH 7.4).

Vesicles were resuspended in a 10 mm quartz cuvette to a concentration of 20 μM (40 μM) in 10 mM Tris and 130 mM KCl (pH 7.4). Melittin was added by injection of a stock solution under rapid mixing. The release of dye from vesicles

[1] Abbreviations: POPC, 1-palmitoyl-2-oleoyl-*sn*-glycero-3-phosphocholine; POPG, 1-palmitoyl-2-oleoyl-*sn*-glycero-3-phosphoglycerol; CD, circular dichroism; ITC, isothermal titration calorimetry; LUV, large unilamellar vesicle; HS, heparan sulfate.

was monitored using an excitation wavelength of 494 nm and an emission wavelength of 517 nm. The intensity was monitored for ~8−10 min. The intensity value for 100% lysis was obtained by injection of 100 μL of a 5% Trition X-100 solution. The measurements were performed at different peptide concentrations to produce different peptide:lipid molar ratios.

Circular Dichroism Spectroscopy. CD measurements of melittin and [D]-$V^{5,8}$,I^{17},K^{21}-melittin in the absence and presence of small unilamellar lipid vesicles [buffer of 25 mM Tris and 50 mM NaF (pH 7.4)] at different temperatures were taken using a Chirascan CD spectrometer (Applied Photophysics Ltd., Leatherhead, U.K.). A quartz cuvette with a path length of 0.1 cm was used. All spectra were corrected by subtracting the buffer or buffer with lipid baseline. The percentage of peptide secondary structure was estimated from a computer simulation based on the reference spectra obtained by Reed and Reed (*18*).

Binding Model. The analysis of the binding isotherm combines electrostatic attraction with a chemical partition equilibrium and has been described previously (*10, 12, 19*). The anionic membrane has a surface potential, ψ, which attracts the cationic peptide with charge z_p. The peptide surface concentration, c_M, is thus larger than the bulk equilibrium concentration, c_{eq}. The ion distribution follows the Boltzman equation

$$c_M = c_{eq} e^{-z_p F_0 \psi / RT} \quad (1)$$

where F_0 is the Faraday constant and RT is the thermal energy.

All measurements are taken in 25 mM Tris buffer containing 50 mM NaCl (with a few experiments at 100 mM NaCl), and the surface potential (ψ) is approximately −45 mV in the absence of peptide. The ζ potential reports the surface potential ~2 Å from the surface.

Peptide binding is a chemical adsorption process and is described here by a surface partition equilibrium

$$X_b = K_0 c_M = K_0 c_{eq} e^{-z_p F_0 \psi / RT} \quad (2)$$

where X_b quantifies the extent of binding [$X_b = n_b/n_{lip}^0 = c_b/c_L^0$ with n_b (c_b) and n_{lip}^0 (c_L^0) denoting the molar amounts (concentrations) of bound melittin and total lipid, respectively]. Binding is defined as a nonspecific adsorption of melittin to the membrane surface.

In the electrophoretic experiments, X_b reaches a maximum value of ≈0.07, that is, seven melittin molecules per 100 lipid molecules. Under these conditions, the charge of the bound peptide exceeds the lipid charge and the ζ potential becomes positive. At the point of charge reversal ($\psi = \zeta = 0$), the surface concentration, c_M, is identical with the bulk equilibrium concentration, c_{eq}. This allows a straightforward estimate of binding constant K_0. The approach pursued here is, however, more comprehensive and provides a quantitative description of the full binding isotherm either in the form $\zeta = f(c_p^0/c_L^0)$ or $X_b = f(c_p^0/c_L^0)$ (c_p^0 and c_L^0 are the total peptide and lipid concentrations, respectively). The unknown parameters in the equation given above are the binding constant, K_0, the equilibrium concentration of melittin, c_{eq}, and the membrane surface potential, ψ. The purpose of our experiments is then to determine K_0 from the experimental parameters ζ and X_b. K_0 is independent of the experimental conditions and provides the free energy, ΔG^0, of the chemical adsorption step. Two additional boundary conditions are helpful. First, the concentrations of bound and free peptide add up to the total protein concentration

$$c_b + c_{eq} = X_b c_L^0 + c_{eq} = c_p^0 \quad (3)$$

Second, the membrane surface potential ψ is intimately connected with the membrane surface charge density σ via the Gouy−Chapman theory (cf. refs *20* and *21*).

$$\sigma^2 = 2000 \varepsilon_0 \varepsilon_R RT \sum_i C_{i,eq} (e^{-z_i F_0 \psi_0 / RT} - 1) \quad (4)$$

where ε_0 is the permittivity of free space, ε_R the relative dielectric constant, and $c_{i,eq}$ the concentration of the ith electrolyte in the bulk aqueous phase. The membrane surface charge density, in turn, is connected with the degree of binding (*12*):

$$\sigma = (e_0/A_L)(-X_{PG} + X_b z_p)/[1 + X_b(A_p/A_L)] \quad (5)$$

where X_{PG} is the mole fraction of anionic PG; $A_L \approx 68$ Å^2 is the surface area per lipid, assumed to be identical for POPC and POPG. e_0 is the elementary electrical charge. A_p (150 Å^2) and z_p (≈3.9−4.4) are the effective area and valency, respectively, of melittin at the membrane surface.

As an additional refinement, the model takes into account Na^+ binding. Na^+ binds to negatively charged phosphatidylglycerol with a binding constant K_{Na^+} of 0.6 M^{-1} (*22*). Binding is saturable and follows the Langmuir adsorption isotherm (*19*). The extent of Na^+ binding is generally small. Finally, the model also considers the pH change near the membrane surface (*19*). The anionic membrane attracts protons, and the pH profile near the plane of binding is again determined by the Boltzmann distribution. In the absence of peptide, the pH for the lipid system investigated here is reduced from pH 7.4 in bulk solution to pH 6.6 near the anionic membrane surface. As the N-terminal amino groups of many peptides have pK values of ≈7.2, the charge z_p of the peptide is not constant but will increase. This effect is also included in the model. No analytical solution in closed form can be given. Numerical solutions are generally found by systematically varying K_0 and ψ until a consistent solution is found for eqs 2−5.

RESULTS

Calcein Release Assay. The experiments show an almost linear increase in calcein leakage as a function of the melittin:lipid ratio, starting at a melittin:lipid ratio as low as 1:1000. This agrees with earlier studies (cf. Figure 3 in ref *23*). Calcein release appears not to be coupled to melittin aggregation on the membrane surface as discussed below. Indeed, much lower melittin concentrations are sufficient for calcein leakage than for membrane-induced melittin aggregation. It was also demonstrated that melittin and [D]-$V^{5,8}$,I^{17},K^{21}-melittin have similar membrane permeating activity with PC/PS vesicles (*17*).

ζ Potential and Vesicle Size. ζ potential measurements were taken with 100 nm POPC/POPG (3:1) vesicles (30 °C; 25 mM Tris, 50 mM NaCl, pH 7.4), and the ζ potential was

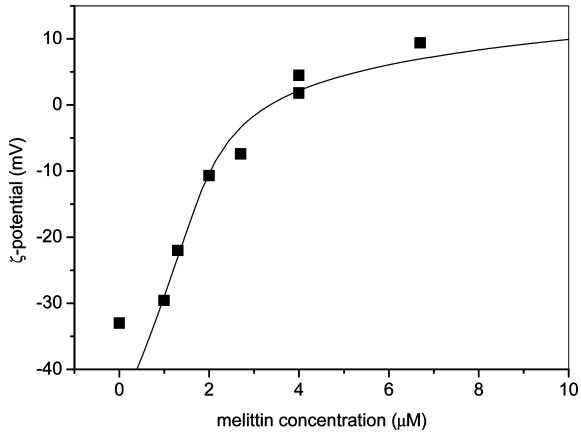

FIGURE 1: ζ potential of POPC/POPG vesicles (3:1 molar ratio, d = 100 nm) as a function of melittin concentration. The total lipid concentration (c^0_{lipid}) is 40 μM, and increasing amounts of melittin are added. The peptide concentrations listed are the total peptide concentrations. The solid line was calculated with a surface partition equilibrium, $X_b = K_0 c_M$, where the surface concentration of melittin, c_M, was calculated with the Gouy−Chapman theory ($K_0 = 6 \times 10^4$ M^{-1}; 25 mM Tris, 50 mM NaCl, pH 7.4, 30 °C).

in the range of −33.0 mV (no melittin) to 9.4 mV (mel:lipid ratio of 0.168) (Figure 1). Electrical neutrality ($\zeta = 0$) was observed at a (total) melittin:(total) lipid ratio of 0.078. As the POPG content of the lipid vesicles is 25%, the peptide charge (z_p) must be at least 0.25/0.078 = 3.2 to achieve charge neutralization. This number defines a lower limit for the peptide charge if indeed all melittin is tightly bound to the lipid membrane. However, some melittin remains always in solution in a thermodynamic equilibrium, and the true peptide charge must be larger than 3.2.

The solid line in Figure 1 is the best fit to the experimental data, using the surface partition model in combination with the Gouy−Chapman theory as described above. The Gouy−Chapman theory predicts a peptide charge between ≈4.4 (low melittin concentration, $\Psi < 0$, pH 6.6 at the membrane surface) and ≈3.9 (high melittin concentration, $\Psi > 0$, pH 7.6 at the membrane surface) (at 30 °C). Electrical neutrality ($\Psi = 0$ mV) is predicted for $c_{eq} = c_M = 1.02$ μM, $X_b = 60$ mmol/mol, and $z_p = 4$. In addition, Na^+ binding is given by $X_{Na^+} = 10$ mmol/mol. The binding constant for binding of melittin to the lipid membrane (K_0) is 6×10^4 M^{-1}.[2])

The binding constant K_0 describes the peptide transfer from the membrane surface to the membrane. The corresponding free energy can be calculated according to

$$\Delta G^0_{exp} = -RT \ln(55.5 K_0) \quad (6)$$

where the factor 55.5 is the molar concentration of water and corrects for the cratic contribution. Numerical results are listed in Table 1.

The ζ potential measurements described in Figure 1 relate to melittin (bound):lipid ratios in the range of 0−70 mmol/mol. Simultaneous size measurements showed a constant vesicle size of 110 ± 8 nm over the whole concentration range. Under the conditions described above, the vesicles are not dissolved or disrupted by melittin, even though they are rather leaky for calcein.

For the analysis of the binding isotherms derived either from ζ potential or from ITC data, we assume a fast translocation of melittin across the lipid membrane. Conflicting views exist about this process. Some authors suggest that melittin will not permeate the membrane at low melittin concentrations (*24*−*27*). This is contrasted with fluorescence measurements indicating pore formation even at low peptide-to-lipid ratios. Pore disintegration was seen to be coupled to melittin translocation across the bilayer (*28*). In this study, all data are consistent with a rapid flip-flop of melittin across the membrane.

Binding Enthalpies of Melittin and [D]-V^{5,8},I^{17},K^{21}-Melittin. In a typical peptide binding experiment, lipid vesicles (∼100 nm diameter; $c^0_{lipid} \sim 10-20$ mM) are injected into a melittin solution ($c^0_{pep} \sim 10-20$ μM) (L-to-P titration). During the first lipid injections, melittin covers a large fraction of the lipid surface, facilitating rapid equilibration of melittin across the bilayer membrane. Each injection generates a heat peak, h_i, which decreases in size with consecutive injections as the supply of melittin is gradually exhausted by binding to the lipid membrane. The molar heat of reaction, ΔH^0_{exp}, can then be calculated as $\sum_i h_i / n^0_p$, where n^0_p denotes the molar amount of peptide in the calorimeter cell.

We also performed peptide-into-lipid (P-to-L) titrations and used melittin concentrations of ∼200 μM in the injection syringe. It was hence necessary to take into account melittin dilution effects. The heat of dilution is small at temperatures between 10 and 30 °C but is considerably larger for higher temperatures. After correction for dilution effects, the reaction enthalpies are identical or similar to those of the L-to-P titration. For both types of titrations, the evaluation of the reaction enthalpy, ΔH^0_{exp}, does not require the assumption of a specific binding model.

Table 1 and Figure 2 summarize the reaction enthalpy, ΔH^0_{exp}, observed for melittin.

ΔH^0_{exp} is endothermic below 28 °C and becomes exothermic above this temperature. The regression analysis yields the following temperature dependencies and molar heat capacity changes:

$$\Delta H^0_{exp}(\text{kcal/mol}) = -0.400x + 11.06 \ (10-30\ ^\circ\text{C})$$
$$= -0.194x + 4.81 \ (30-60\ ^\circ\text{C})$$

where x denotes the temperature in degrees Celsius and the slopes define the molar heat capacity change, $\Delta C^0_{p,exp}$. At ∼28 °C, the reaction enthalpy is zero. In addition to Tris buffer, we have measured melittin binding also in phosphate and HEPES. Within the accuracy of the measurement, we obtain the same ΔH^0_{exp} for all three buffers.

Analogous ITC experiments were performed with [D]-V^{5,8},I^{17},K^{21}-melittin. In this molecule, the replacement of L-amino acids with their stereoisomers inhibits α-helix formation. This is clearly reflected in the ITC results summarized as ΔH^0_{d4mel} in Table 2 and Figure 2. The binding enthalphies are always endothermic (except at 60 °C) and are larger by ∼7 kcal/mol compared to those of melittin. This remarkable difference can be explained by

[2] We have previously determined the binding constant of melittin to sonified small unilamellar POPC/POPG vesicles 30 nm in diameter using circular dichroism spectroscopy. The binding constant (K_0) was $(4.5 \pm 0.6) \times 10^4$ M^{-1}, in agreement with the analysis presented here (*12*). The calculation was performed with a fixed peptide charge (z_p) of 2.2. In terms of a variable peptide charge caused by pH changes, the reanalysis of the earlier data yields a z_p of ≈3.1−2.8.

Table 1: Isothermal Titration Calorimetry, ζ Potential Measurements, and CD Spectroscopy of Melittin

Isothermal Titration Calorimetry										
temp (°C)	ΔH^0_{exp} (kcal/mol)	K_0[a] (M^{-1})	ΔG^0_{exp}[b] (kcal/mol)	$T\Delta S^0_{exp}$ (kcal/mol)	ΔS^0_{exp} (cal mol^{-1} K^{-1})	ΔH^0_{agg} (kcal/mol)	$z_{(\zeta=0)}$[c]	α-helix[d] (%)	β-structure[d,e] (%)	random coil[d](%)
50 mM NaCl and 25 mM Tris (pH 7.4)										
10	6.3 ± 1.0	4.00×10^4	−8.2	14.5 ± 1	51.2 ± 3.6	2.34 ± 0.53	4	67	16	17
20	3.5	5.50×10^4	−8.7	12.2	41.6	1.4	4	64	23	14
25	1.0	6.00×10^4	−8.9	9.9	33.1	1.8	4	63	17	20
27	0.2	6.05×10^4	−8.9	9.1	30.4	1.3	4			
28	0.0	6.05×10^4	−9.0	9.0	29.8	1.6	4	60	18	20
30	−1.15 ± 0.15	6.00×10^4	−9.0	7.95 ± 0.15	26.25 ± 0.45	1.75 ± 0.05	4	59	19	22
35	−2.6	5.50×10^4	−9.1	6.5	21.1	2.1	4	56	20	24
37	−2.6	5.00×10^4	−9.1	6.5	20.9	1.7	4			
40	−3.4	5.00×10^4	−9.2	5.8	18.4	1.5	4	54	21	25
50	−5.2	4.60×10^4	−9.4	4.2	13	1.1	4	51	22	28
60	−6.7	3.30×10^4	−9.5	2.9	8.6	1.1	4	47	23	30
100 mM NaCl and 25 mM Tris (pH 7.4)										
50	−3.49	6.00×10^4	−9.0	6.1	18.9	0.8	3.5			

ζ Potential Measurements						
	$c^0_{melittin}$ (μM)	c^0_{lipid} (μM)	K_0[a] (M^{-1})	ζ potential (mV)	z_p	pH[f]
50 mM NaCl and 25 mM Tris (pH 7.4)						
30	1	40	6.00×10^4	−33	4.4	6.6
30	6.7	40	6.00×10^4	9.4	3.9	7.6

[a] Binding constant of the surface partition equilibrium $X_b = K_0 c_M$, where c_M is the melittin surface concentration. [b] ΔG^0_{exp} was calculated according to the relationship $\Delta G^0 = -RT \ln(55.5K_0)$, where 55.5 is the molar concentration of water and accounts for the cratic contribution. [c] Effective melittin charge under conditions where the ζ potential equals zero. The pH at the membrane surface changes during the course of the ITC titration between pH 6.6 (no melittin, negative charge of lipid vesicles) and pH 7.6 (excess melittin over POPG, positive charge at the membrane surface). Accordingly, the melittin charge varies between 4.4 and 3.9 as the N-terminal amino group is assumed to have a p*K* of 7.2. [d] CD spectra of melittin bound to POPC/POPC (3:1) vesicles. [e] Sum of β-sheet and β-turn. [f] pH at the membrane surface.

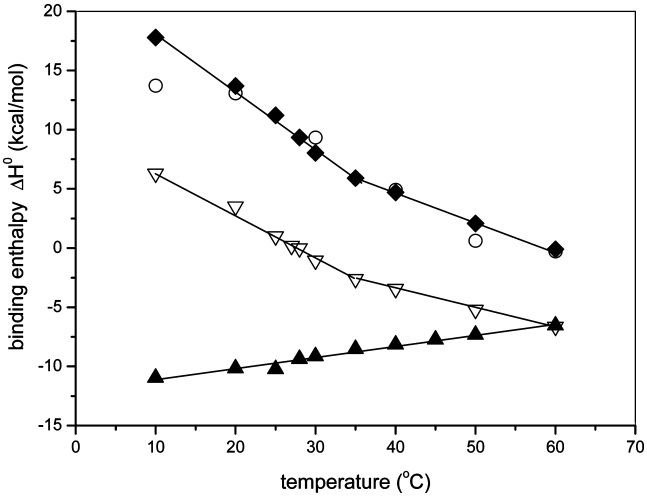

FIGURE 2: Temperature dependence of the measured reaction enthalpies of synthetic melittin, ΔH^0_{exp} (▽), and [D]-$V^{5,8}$,I^{17},K^{21}-melittin, ΔH^0_{d4mel} (○). Also included are the calculated enthalpies of melittin α-helix formation ΔH^0_{helix} (▲) and the binding enthalpy of unstructured melittin, ΔH^0_{bind} (◆). ΔH^0_{exp} and ΔH^0_{d4mel} were measured with isothermal titration calorimetry. ΔH^0_{bind} was calculated according to the relationship $\Delta H^0_{bind} = \Delta H^0_{exp} - \Delta H^0_{helix}$ (25 mM Tris, 50 mM NaCl, pH 7.4).

conformational differences between the two peptides as revealed by circular dichroism spectroscopy and discussed below.

Secondary Structure of Membrane-Bound Melittin and [D]-$V^{5,8}$,I^{17},K^{21}-Melittin. Melittin changes its conformation from mainly random coil in buffer to α-helical when bound to lipid vesicles. To quantify the extent of α-helix formation, we recorded circular dichroism (CD) spectra of melittin in buffer and in the membrane-bound state between 10 and 60 °C. Deconvolution of the spectra provided the relative contributions of the major structural elements which are listed in Table 1. The α-helix content of membrane-bound melittin is in the range of 67% (10 °C) to 47% (60 °C).

The circular dichroism spectra of [D]-$V^{5,8}$,I^{17},K^{21}-melittin in buffer and in its membrane-bound conformation are compared in Figure 3 to that of membrane-bound melittin. The spectra are similar but not identical to those observed in a 40% trifluoroethanol/water mixture (*17*).

The spectrum of [D]-$V^{5,8}$,I^{17},K^{21}-melittin in buffer has the same shape as the melittin spectrum (not shown), but its amplitude is reduced. In [D]-$V^{5,8}$,I^{17},K^{21}-melittin, the optical activity of four L-amino acids is compensated by four D-amino acids. Since the D-amino acids are spread along the chain, they are expected to break the structure of melittin rather than defining a mirror image structure as anticipated for four consecutive D-amino acids. Therefore, only the remaining 18 L-amino acids determine the net spectrum. Indeed, if the amplitudes of the melittin spectrum are reduced by a factor of 18/26, the reduced spectrum exactly matches the experimental [D]-$V^{5,8}$,I^{17},K^{21}-melittin spectrum.

In contrast, the two peptides exhibit circular dichroism spectra of quite different shape when bound to lipid membranes (Figure 3). Normalizing the melittin spectrum by a factor *f* of 18/26 does not generate the [D]-$V^{5,8}$,I^{17},K^{21}-melittin spectrum. Instead, deconvolution after intensity correction yields 38% random coil, 34% β-sheet, 19% β-turn, and 9% α-helix for [D]-$V^{5,8}$,I^{17},K^{21}-melittin at 20 °C (cf.

Table 2: Isothermal Titration Calorimetry and CD Spectroscopy of [D]-$V^{5,8}$,I^{17},K^{21}-Melittin Binding to POPC/POPG 100 nm Vesicles [50 mM NaCl and 25 mM Tris (pH 7.4)]

temp (°C)	ΔH^0_{d4mel} (kcal/mol)	K_0[a] (M^{-1})	ΔG^0_{d4mel}[b] (kcal/mol)	$T\Delta S^0_{d4mel}$ (kcal/mol)	ΔS^0_{d4mel} (cal mol^{-1} K^{-1})	ΔH^0_{agg} (kcal/mol)	$z_{(\zeta=0)}$[c]	α-helix (%)[d]	β-structure (%)[d,e]	random coil (%)[d]
					Buffer Only					
25									29	71
					Membrane-Bound					
10	13.3	100	−4.8	18.2	64.1	−1.6	4.2	16	55	28
20	13.3	200	−5.4	18.7	63.8	−3.4	4.2	9	53	38
28								6	54	40
30	9.4	480	−6.1	15.5	51.1	−2.4		5	55	41
35								4	54	42
40	4.9	710	−6.6	11.4	36.5	−0.94	4.2	5	52	43
50	1.7	840	−6.9	8.5	26.4	0.14	4.1	3	52	44
60	−0.3	800	−7.1	6.8	20.3	0.37	4.1	2	52	46

[a] Binding constant of the surface partition equilibrium $X_b = K_0 c_M$, where c_M is the melittin surface concentration. [b] ΔG^0_{exp} was calculated according to the relationship $\Delta G^0 = -RT \ln(55.5K_0)$, where 55.5 is the molar concentration of water and accounts for the cratic contribution. [c] Effective melittin charge at a peptide equilibrium concentration (c_{eq}) of 1 μM. The pH at the membrane surface changes during the course of the ITC titration between pH 6.6 (no melittin) and pH 7.2 ($X_b \sim 45$ mmol/mol). Accordingly, the melittin charge varies between 4.4 and 3.9 as the N-terminal amino group is assumed to have a pK of 7.2. Because of the lower binding constant of [D]-$V^{5,8}$,I^{17},K^{21}-melittin, the surface potential always remains negative. [d] CD spectra of melittin bound to POPC/POPC (3:1) vesicles. [e] Sum of β-sheet and β-turn.

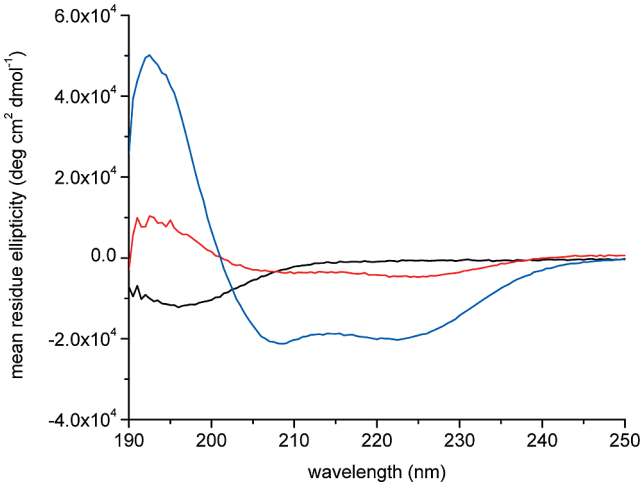

FIGURE 3: Circular dichroism spectra of [D]-$V^{5,8}$,I^{17},K^{21}-melittin in buffer (black), membrane-bound [D]-$V^{5,8}$,I^{17},K^{21}-melittin (red), and membrane-bound melittin (blue). POPC/POPG (3:1) small unilamellar vesicles 30 nm in diameter in 25 mM Tris and 50 mM NaF (pH 7.4), at 25 °C.

Table 2). Very little α-helix but 50−55% β-structure is found for membrane-bound [D]-$V^{5,8}$,I^{17},K^{21}-melittin, whereas the α-helix content of melittin under the same conditions is 63%. This is different from NMR studies of [D]-$V^{5,8}$,I^{17},K^{21}-melittin in a micellar environment indicating ~30% α-helix (*3*). These conformational differences have important consequences for the thermodynamical parameters.

Binding Constants and Free Energy of Binding. The ITC experiment can be used to construct the binding isotherm as described previously for the related peptides magainin 2 and PGLa (*19*, *29*−*31*; cf. also ref *32*). The binding isotherm can then be analyzed in terms of the model discussed above to deduce the binding constant K_0. Figure 4A shows the binding constant of melittin as a function of temperature, and numerical data are listed in Table 1. We note that isothermal calorimetry and ζ potential measurements lead to the same binding constant ($K_0 = 6 \times 10^4$ M^{-1}) at 30 °C and peptide charge ($z_p = 3.9$−4.4) (depending on the pH near the membrane surface). The binding constants of [D]-$V^{5,8}$,I^{17},K^{21}-melittin were deduced exclusively from ITC measurements and are summarized in Table 2 and Figure 4B. The peptide charge is found to be very similar ($z_p = 4.2$) to that of melittin. However, the binding constants of [D]-$V^{5,8}$,I^{17},K^{21}-melittin are ~2 orders of magnitude smaller than those of melittin at corresponding temperatures. In addition, the maximum is shifted by ~20 °C toward higher temperatures.[3] The solid lines in both figures correspond to the theoretical temperature dependence, calculated with van't Hoff's law and the temperature-dependent enthalpy values ΔH^0_{exp} and ΔH^0_{d4mel} displayed in Figure 2.

The Gibbs free energies of melittin, ΔG^0_{exp}, and of [D]-$V^{5,8}$,I^{17},K^{21}-melittin, ΔG^0_{d4mel}, can be calculated from the binding constants (eq 6) and are displayed in Figure 5.

The α-helix-forming melittin binds better to membranes by approximately −3.5 to −2.5 kcal/mol than the nonhelical [D]-$V^{5,8}$,I^{17},K^{21}-melittin. The difference can be explained by calculating the contribution of α-helix formation to binding (cf. below).

Pore Formation. In addition to binding and α-helix formation, melittin aggregation is a third process which contributes to the thermodynamic parameters. This is particularly obvious in Figure 6B where the ITC experiment was performed at 28 °C. Endothermic and exothermic heat flows, h_i, offset each other, and consequently, the binding enthalpy is zero ($\Delta H^0_{exp} = 0$).

The observed heats of reaction are caused by a process which is only indirectly related to binding. This reaction is interpreted as aggregation/pore formation of melittin.

An endothermic process takes place during the initial phase of the titration where the peptide-to-lipid ratio is largest. Vesicles covered with aggregated melittin are formed first. Then, as more lipid is injected, the membrane-bound aggregates gradually disintegrate, returning the heat of aggregation in an exothermic reaction.

The aggregation−dissociation reaction can also be seen at other temperatures. However, it is then superimposed on

[3] Earlier measurements of [D]-$V^{5,8}$,I^{17},K^{21}-melittin report a K_0 of (1.1 ± 0.2) × 10^4 M^{-1} by fluorescence spectroscopy (*17*) or a K_x of 80 ± 30 by equilibrium dialysis (*13*). K_x must be divided by 55.5 to be comparable with K_0 as defined here or in ref *17*. Electrostatic effects were not considered in the analysis of the binding data.

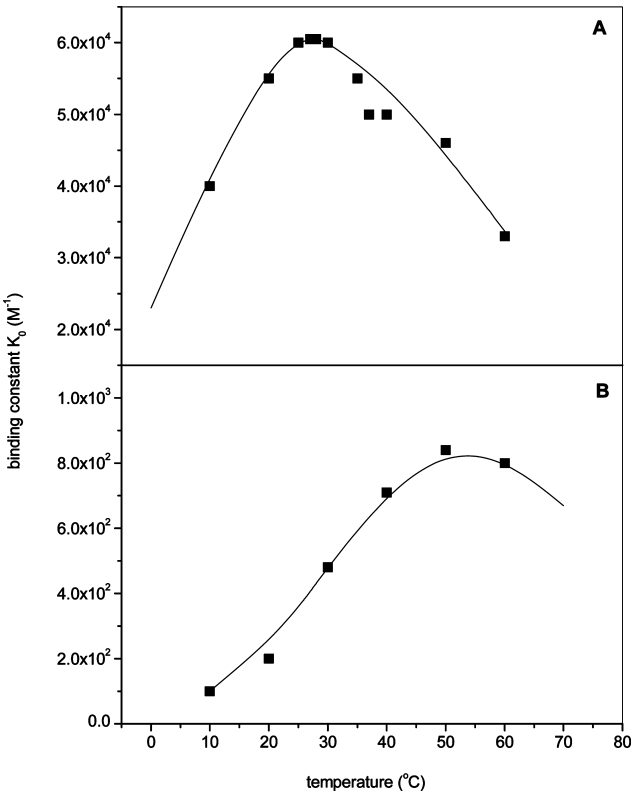

FIGURE 4: Temperature dependence of binding constant K_0 (after correction for electrostatic attraction) of synthetic melittin (A) and [D]-$V^{5,8}$,I^{17},K^{21}-melittin (B) both binding to POPC/POPG (3:1) unilamellar vesicles 100 nm in diameter. The solid lines are the theoretical binding curves based on van't Hoff's law and calculated with the temperature-dependent reaction enthalpies ΔH^0_{exp} and ΔH^0_{d4mel}, respectively, of Figure 2.

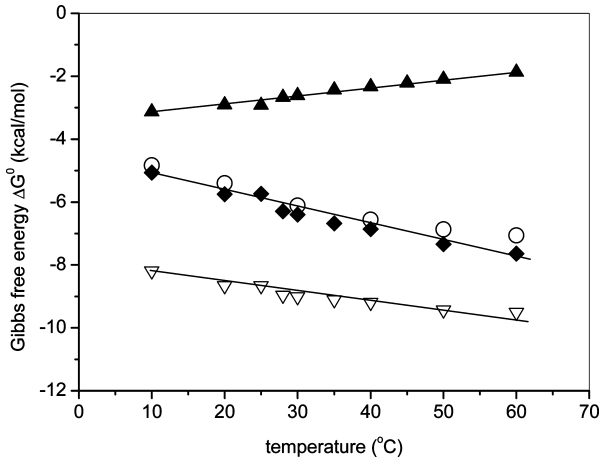

FIGURE 5: Gibbs free energy, calculated according to the relationship $\Delta G^0 = -RT \ln(55.5K_0)$ for the binding of synthetic melittin, ΔG^0_{exp} (▽), and [D]-$V^{5,8}$,I^{17},K^{21}-melittin, ΔG^0_{d4mel} (○). Also included is the calculated free energy of helix formation, ΔG^0_{helix} (▲), of melittin and $\Delta G^0_{bind} = \Delta G^0_{exp} - \Delta G^0_{helix}$ (◆), the binding energy of unstructured melittin.

the binding enthalpies proper. The aggregation−dissociation reaction can be easily detected by eye for temperatures below 28 °C (cf. Figure 6A). On the other hand, at 50 and 60 °C, the binding enthalpies are too large, and the ITC curves look smooth (Figure 6C). Only the comparison with the theoretical ITC curve reveals the aggregation−dissociation process with its endothermic and exothermic deviations from the theoretical prediction.

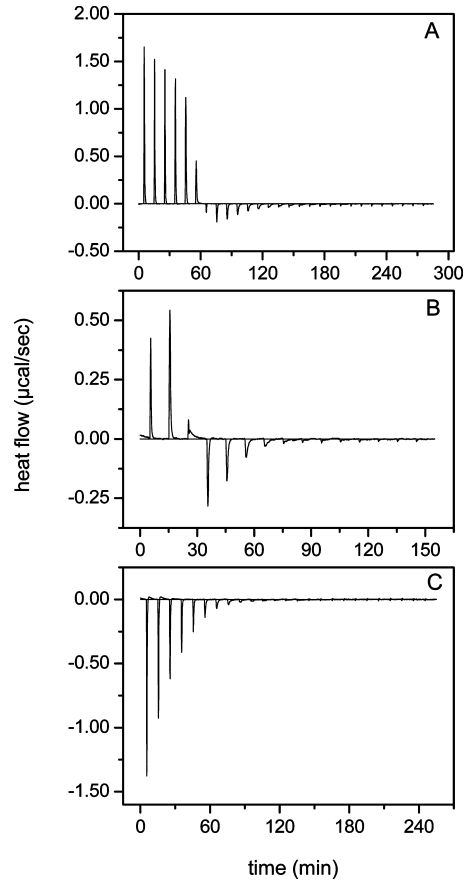

FIGURE 6: Isothermal titration calorimetry with synthetic melittin and LUVs. Melittin in buffer is titrated with 100 nm unilamellar POPC/POPG (3:1) vesicles in the same buffer. The experiment was performed at (A) 10, (B) 28, and (C) 50 °C. The experimental binding enthalpy (ΔH^0_{exp}) at 28 °C is zero, and the endothermic peaks of the first phase are exactly compensated by the exothermic peaks of the second phase of the titration [25 mM Tris and 50 mM NaCl (pH 7.4)].

Each of the two halves of the titration curve shown in Figure 6B yields the enthalpy of aggregation/pore formation, ΔH_{agg}. The cumulative heat after three injections is 44.7 μcal and the amount of bound peptide 24 nmol. If one assumes that all bound peptide is aggregated, then the reaction enthalpy of aggregation (ΔH^0_{agg}) equals 1.86 kcal/mol. Analysis of the titration curves at other temperatures reveals a small temperature dependence according to

$$\Delta H^0_{agg}(\text{kcal/mol}) = -0.0165x + 2.32$$

with a negative heat capacity change $\Delta C_{p,agg}$ of −16.5 cal mol^{-1} K^{-1}.

We have performed calorimetric titrations at peptide concentrations between 19.7 and 49.7 μM (at 10 °C). No systematic change in ΔH^0_{agg} with an increase in peptide concentration was observed. The average enthalpy ΔH^0_{agg}(10 °C) was 2.34 ± 0.53 kcal/mol.

The aggregation phenomenon is also observed for ITC measurements with [D]-$V^{5,8}$,I^{17},K^{21}-melittin, and the corresponding data are listed in Table 2. The temperature dependence can be described by the relationship ΔH^0_{agg}(kcal/mol) = $0.10x - 5.28$.

Phase Diagram of Melittin Aggregation. Depending on the experimental conditions, the lipid membrane may contain only monomers, a mixture of monomers and aggregates, or

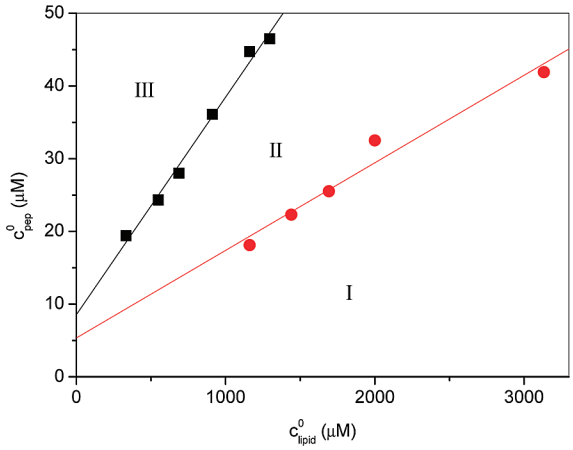

FIGURE 7: Approximate phase diagram for melittin aggregation in the lipid phase at 10 °C. The onset and the end of melittin aggregation in the lipid phase were determined from the calorimetric titration curves, and the corresponding total peptide, c^0_p, and total lipid concentration, c^0_L, were determined. In region I, only melittin monomers exist. In region II, monomers are in equilibrium with aggregates. Region III defines the existence range of aggregates.

only aggregates. The boundaries between these three phases can be deduced with ITC measurements performed at different melittin concentrations. Here we report lipid-into-peptide titration at 10 °C with melittin concentrations in the range of 20−50 μM. The phase boundaries are determined by a comparison of the measured binding isotherm with the theoretical prediction. For a given peptide concentration, c^0_p, in the calorimeter cell, those two lipid concentrations, c^0_L, are determined where the experimental titration curve intersects the theoretical binding isotherm. A simple procedure can then be applied to construct an approximate phase diagram (*29, 33*). The total peptide concentration in the calorimeter cell, c^0_p, can be divided into bound peptide, c_b, and peptide at equilibrium free in solution, c_{eq}.

$$c^0_p = c_b + c_{eq}$$

In the simplest case, if we neglect charge effects, the binding reaction follows a partition equilibrium.

$$X_b = \frac{c_b}{c^0_L} = Kc_{eq}$$

Peptide aggregation on the membrane surface starts at a critical ratio X^*_b, and the critical concentration of bound peptide is

$$c^*_b = X^*_b c^0_L$$

leading to the following expression for the total peptide concentration

$$c^0_p = X^*_b c^0_L + c^*_{eq}$$

A plot of the total peptide concentration versus the corresponding total lipid concentration at the onset and end of aggregation yields the respective phase boundary with slope X^*_b. Figure 7 shows this plot for the two boundaries discussed above, yielding an X^*_b of ≈37 ± 7 mmol/mol for the boundary of the aggregate−aggregate monomer coexistence phase and an X_b of ≈13 ± 4 mmol/mol for the aggregate monomer coexistence−monomer phase boundary.

The straight lines in Figure 7 should intersect the ordinate at c^*_{eq}. In these experiments, it is difficult to evaluate c^*_{eq} correctly as the scatter of the experimental data is considerable. In addition, electrostatic effects were neglected, and on the basis of the Gouy−Chapman analysis, the straight lines are predicted to intersect the ordinate closer to the origin than deduced from linear regression analysis of the data shown in Figure 7.

On the basis of neutron diffraction and CD spectroscopy, Huang and co-workers found thresholds for pore formation of melittin in the P-to-L range of 1:30 to 1:100, using supported lipid bilayers. Concomitantly, the melittin molecule changed its orientation from parallel to perpendicular to the bilayer surface (*6, 34*). The experimental conditions of these earlier studies are not exactly comparable to those used to collect the data presented here; nevertheless, the critical phase boundaries discussed in ref *34* are in agreement with our results.

DISCUSSION

α-Helix and β-Structure Formation of Membrane-Induced Peptide Folding Contribute Differently to Binding. Melittin and [D]-V^{5,8},I^{17},K^{21}-melittin adopt different conformations upon binding to POPC/POPG membranes. Melittin is 60% α-helical with 18% β-structure, and [D]-V^{5,8},I^{17},K^{21}-melittin is 5% α-helical with 55% β-structure (at 28 °C). The thermodynamic parameters as derived from the ITC experiments are distinctly different. In the following, we demonstrate that the thermodynamic differences can be explained by general rules derived for membrane-induced peptide folding (*30, 31, 35*).

We have shown previously for the antibacterial peptide magainin 2 and for the presequence of rat mitochondrial rhodanese that membrane-induced α-helix formation is an exothermic reaction with an h_{helix} of −0.7 to −0.8 kcal/mol and is energetically favorable with a g_{helix} of −0.14 to −0.20 kcal/mol per amino acid residue (*30, 31*).[4] As the extent of α-helix formation for melittin is known, the corresponding enthalpy and free energy contributions can be calculated as

$$\Delta H^0_{helix} = n\Delta\Theta_{helix}h_{helix} \quad (7)$$

$$\Delta G^0_{helix} = n\Delta\Theta_{helix}g_{helix} \quad (8)$$

$n = 26$ is the length of melittin in terms of amino acids and $\Delta\Theta_{helix}$ is the fractional change in α-helix content upon membrane binding. The results of these calculations are displayed in Figure 2 for ΔH^0_{helix} and in Figure 5 for ΔG^0_{helix}. ΔH^0_{helix} increases from −11.0 kcal/mol at 10 °C to −6.5 kcal/mol at 60 °C using an h_{helix} of −0.7 kcal/mol. In parallel,

[4] α-Helix formation of melittin can also be induced by different alcohols. The free energy change, ΔG_w, for converting one residue from coil to α-helix was determined for a series of alcohols (*44*). ΔG_w (= g_{helix} in the present notation) at maximum α-helix formation was approximately −0.19 kcal/mol. From the thermodynamics of a fusion peptide, Li et al. (*45*) estimated a g_{helix} of −0.25 ± 0.05. Ladokhin and White (*13*) measured a free energy change g_{helix} of −0.4 kcal/mol for the folding of melittin in membranes. This latter value is probably too high as the binding constant of [D]-V^{5,8},I^{17},K^{21}-melittin was largely underestimated.

$\Delta G^0_{\text{helix}}$ increases from −3.1 to −1.9 kcal/mol in the same temperature interval ($g_{\text{helix}} = -0.2$ kcal/mol). Next, the experimental values of ΔH^0_{exp} and ΔG^0_{exp} are corrected for α-helix formation, yielding the binding parameters of the binding step proper, that is, melittin binding without peptide folding:

$$\Delta H^0_{\text{bind}} = \Delta H^0_{\text{exp}} - \Delta H^0_{\text{helix}} \quad (9)$$

$$\Delta G^0_{\text{bind}} = \Delta G^0_{\text{exp}} - \Delta G^0_{\text{helix}} \quad (10)$$

The results of these calculations are included in Figure 2 for the enthalpy [ΔH^0_{bind} (◆)] and in Figure 5 for the free energy [ΔG^0_{bind} (◆)]. We obtain the at first sight unexpected result that the binding thermodynamics of unfolded (hypothetical) melittin (◆) is identical to that of β-structured [D]-V^{5,8},I^{17},K^{21}-melittin (○) for which no conformational correction was made. However, in view of recent results with β-structured model peptides, this result is not surprising. The change from random coil to β-structure has much smaller thermodynamic consequences than the random coil to α-helix transition (*36, 37*). For sufficiently large peptide chains with ≥18 amino acid residues, the conformational change is associated with an enthalpy change (h_β) of −0.23 kcal/mol and a free energy change (g_β) of −0.15 kcal/mol per residue (*36*). However, for shorter peptide sequences, these values move close to zero or even become positive (*37*). For [D]-V^{5,8},I^{17},K^{21}-melittin, the conformational change involves a short stretch of eight to nine amino acid residues, and the corresponding enthalpy and free energy contributions must therefore be close to zero. The experimentally measured values of $\Delta H^0_{\text{d4mel}}$ and $\Delta G^0_{\text{d4mel}}$ thus report the binding step proper of [D]-V^{5,8},I^{17},K^{21}-melittin as the conformational change makes no contribution. The quantitative comparison of the melittin/[D]-V^{5,8},I^{17},K^{21}-melittin peptide pair thus provides independent and important support for the general validity of the thermodynamic parameters for membrane-induced α-helical and β-structured folding of amphipathic peptides deduced previously and listed above.

Binding without Folding. The analysis given above demonstrates that the thermodynamics of the melittin binding step can be separated from melittin folding. The results are displayed in Figures 2 and 5 by ΔH^0_{bind} and ΔG^0_{bind}. Inspection of Figure 2 reveals that ΔH^0_{bind} is endothermic over the whole temperature range. The driving force for membrane insertion is thus the hydrophobic effect. At 28 °C, $\Delta H^0_{\text{bind}} = 9.4$ kcal/mol and $\Delta G^0_{\text{bind}} = -6.3$ kcal, leading to a large positive entropy change $T\Delta S^0_{\text{bind}}$ of 15.7 kcal/mol and a ΔS^0_{bind} of 52 cal mol^{-1} K^{-1}. The hydrophobic effect is usually explained by the loss of hydration water as the amphipathic molecule enters the lipid bilayer. This is supported by the large negative heat capacity change ΔC^0_p of −200 to −400 cal mol^{-1} K^{-1} which is also characteristic of the hydrophobic effect.

The binding enthalpy ΔH^0_{bind} can be analyzed further in terms of polar and apolar enthalpy contributions for the interaction of melittin with the lipid membrane. The analysis is based on the parameter set provided in ref *38*. The accessible surface area of melittin based on its molecular weight is $A_S = 11.12M^{2/3} = 2235$ Å^2 (*39*). If 1550 Å^2 (∼70%) is buried in the nonpolar region of the membrane and if this surface area is composed of apolar (75%) and polar (25%) residues, then the calculation agrees with $\Delta C_{p,\text{bind}}$ and ΔH^0_{bind} over the temperature range measured.

Melittin interacts with sulfated cell surface sugars such as heparan sulfate (HS) (*7*). Under conditions comparable to those of the study presented here, the reaction enthalpy $\Delta H^0_{\text{melittin/HS}}$ equals −1.5 kcal/mol and the free energy change $\Delta G^0_{\text{melittin/HS}}$ equals −7.4 kcal/mol (at 28 °C). The molar heat capacity change $\Delta C^0_{p,\text{melittin}}$ equals −227 cal mol^{-1} K^{-1}. These numbers are remarkably close to those found for the interaction with the lipid membrane and again attest to the predominance of the hydrophobic effect. Likewise, the addition of HS to melittin increases the melittin helix content steeply by ∼40%. Applying the same parameters described above, we find the change of 10.4 melittin residues from random coil to α-helix entails an enthalpy change $\Delta H^0_{\text{helix}}$ of −7.2 kcal/mol and a free energy change $\Delta G^0_{\text{helix}}$ of −2 kcal/mol. The binding step without folding is then characterized by a $\Delta H^0_{\text{bind/HS}}$ of 5.7 kcal/mol and a $\Delta G^0_{\text{bind/HS}}$ of −5.4 kcal/mol which may be compared to the $\Delta H^0_{\text{bind/lip}}$ of 9.4 kcal/mol and the $\Delta G^0_{\text{bind/lip}}$ of −6.3 kcal/mol for melittin binding to the lipid phase. The close similarity of the two sets of data suggests that the hydration layer of the membrane surface and around the sulfated sugar HS is very similar, leading to quantitatively similar hydrophobic effects.

Thermodynamics of Melittin Aggregation/Pore Formation. Using selectively deuterated phospholipids, the effect of melittin on the lipid headgroups and hydrocarbon chains was measured with deuterium and phosphorus-31 NMR for neutral and negatively charged lipid bilayers (*10, 12*). The deuterium NMR spectra were characterized by a single quadrupole splitting indicating a time-averaged lipid conformation at all melittin concentrations. No phase separation of the lipids was observed with POPC/POPG vesicles up to X_b of ∼67 mmol/mol. The NMR data thus provide strong evidence for short-lived melittin aggregates with rapid lipid exchange.

This is supported by a quantitative analysis of the free energy of aggregation. As a first approximation, melittin aggregation in the lipid phase (monomer → aggregate) is comparable to micelle formation (monomer → micelle) of detergents in aqueous solutions. The same formalism used for micelle formation can be applied, and the free energy of aggregation ΔG^0_{agg} equals $RT \ln X^*_b$. In addition, the aggregation constant is $K_{\text{agg}} \sim 1/X^*_b$. Insertion of the numerical values given above leads to a ΔG of approximately −2.0 kcal/mol and a K_{agg} of 27 M^{-1}.

The micellar model is a two-state model and neglects intermediates. A more general approach is the isodesmic aggregation model (cf. refs *40*−*42*). The aggregation of melittin is separated into (i) a nucleation step

$$A + A \xrightarrow{\kappa K_{\text{agg}}} A_2$$

and (ii) a growth step

$$\begin{aligned} A_2 + A &\xrightleftharpoons{\text{Kagg}} A_3 \\ \vdots &\quad\quad \vdots \\ A_{n-1} + A &\xrightleftharpoons{\text{Kagg}} A_n \end{aligned}$$

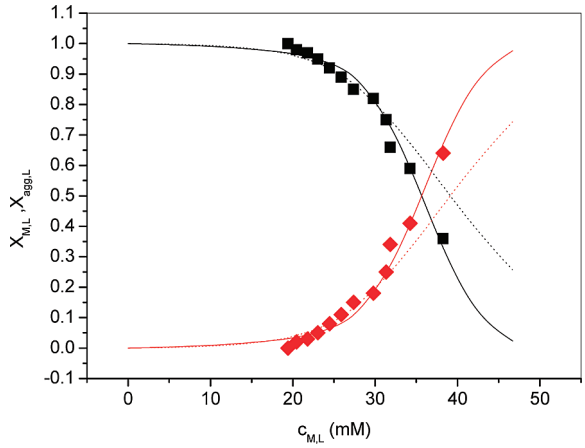

FIGURE 8: Melittin aggregation equilibrium. Melittin monomers and melittin aggregates coexist in the lipid membrane. $X_{M,L}$ denotes the mole fraction of monomers; $X_{agg,L}$ (=1 − $X_{M,L}$) denotes the mole fraction of aggregates (in monomer units). $X_{M,L}$ and $X_{agg,L}$ are plotted as a function of melittin monomer concentration, $c_{M,L}$, in the lipid membrane. The solid line was calculated with the aggregation model described in the text with a maximum aggregate size of $n = 20$. The dashed line corresponds to $n = 6$.

The equilibrium constant K_{agg} describes the addition of a molecule A to an already existing aggregate of length A_i. The formation of a nucleus A_2 is more difficult by a nucleation factor $\kappa < 1$ (negative cooperativity). The aggregation model contains aggregates of all sizes between 2 and n, the relative contribution of which depends on κ, K_{agg}, and n. Mass conservation requires

$$C_A^0 = C_A + 2C_{A_2} + 3C_{A_3} \ldots nC_{A_n}$$

where C_A is the monomer concentration of peptide in the lipid matrix while C_A^0 is the total concentration of peptide in the lipid phase. An analytic expression can be given for this series (*42*). For a given set of parameters κ, K_{agg}, and n, the model provides the fraction of monomers as a function of the monomer peptide concentration, $X_{M,L}$, both referred to the lipid phase. Both $X_{M,L}$ and C_A can be deduced, at least approximately, from the experimental data shown in Figure 6. Considering the dissociation reaction and numbering the exothermic h_i values (right half of Figure 6A) from 1 to n, we can estimate the fraction of monomers in the lipid phase as

$$X_{M,L}^{(i)} = \sum_1^i h_i \Big/ \sum_1^k h_i$$

$\sum_1^k h_i$ corresponds to the total heat of dissociation. The extent of bound peptide, $X_b^{(i)}$, can be calculated with the Gouy−Chapman theory. The concentration of monomeric melittin in the lipid phase, denoted $c_{M,L}$, is then given by

$$c_{M,L}^{(i)} = X_{M,L}^{(i)} X_b^{(i)}/0.8$$

where $X_b^{(i)}$ is defined as $X_b^{(i)} = n_{mel,bound}^{(i)}/n_{lipid}^0$ mol/mol. The partial specific volume of lipid equals that of water with $\tilde{V}_{lipid}$ being approximately 1 mL/g (*43*), and the molecular volume of 1 mol of lipid ∼ 800 g of lipid is thus ∼0.8 L.

Figure 8 then shows the variation of $X_{M,L}$ as a function of $C_{M,L}$. [The first exothermic h_i yields an $X_{M,L}^{(i)}$ of 0.27. However, Figure 6 shows that the dissociation must set in even earlier, and $X_{M,L}^{(i)}$ was corrected to 0.36.] It should be noted that the concentration of melittin in the lipid matrix is in the millimolar range, while it is micromolar in the aqueous phase. The difference is caused by the high binding constant of melittin.

As the experimental data provide no clue about the size of the aggregates, two $n = 6$ and $n = 20$ aggregates were investigated. Both models fit approximately the data, with a somewhat better fit for $n = 20$. The binding constant K_{agg} equals 20 or 38 M^{-1}, and the cooperativity parameter κ = 0.01 or 0.004. The isosdesmic aggregation model and the simpler micelle formation model lead to almost identical binding constants, K_{agg}. As a general conclusion, it follows that melittin aggregation in the lipid phase is a process of low affinity with a K_{agg} of 20−40, a ΔG_{agg}^0 of approximately −1 to −2 kcal/mol, and some negative cooperativity.

Concluding Remarks. Melittin is attracted electrostatically to anionic lipid membranes, but the binding to 100 nm vesicles (which are close to planar membranes) is driven exclusively by the hydrophobic effect. The binding enthalpy of the unstructured melittin is endothermic over the whole measured temperature interval. The folding of melittin into an α-helix is enthalpically favorable and enhances melittin binding by at least 2 orders of magnitude. The thermodynamic analysis is confirmed by comparison with that of [D]-$V^{5,8}$,I^{17},K^{21}-melittin which cannot undergo the random coil-to-α-helix transition. At sufficiently high melittin concentrations, the peptide molecule aggregates on the membrane surface and the approximate phase diagram at 10 °C is deduced. Aggregation is also an entropically driven process, but aggregate formation is weak and lipid exchange rapid. [D]-$V^{5,8}$,I^{17},K^{21}-Melittin also forms aggregates at sufficiently high concentrations.

REFERENCES

1. Habermann, E. (1972) Bee and wasp venoms. *Science 177*, 314–322.
2. Tosteson, M. T., Holmes, S. J., Razin, M., and Tosteson, D. C. (1985) Melittin lysis of red cells. *J. Membr. Biol. 87*, 35–44.
3. Sharon, M., Oren, Z., Shai, Y., and Anglister, J. (1999) 2D-NMR and ATR-FTIR study of the structure of a cell-selective diastereomer of melittin and its orientation in phospholipids. *Biochemistry 38*, 15305–15316.
4. Allende, D., Vidal, A., Simon, S. A., and McIntosh, T. J. (2003) Bilayer interfacial properties modulate the binding of amphipathic peptides. *Chem. Phys. Lipids 122*, 65–76.
5. Stromstedt, A. A., Wessman, P., Ringstad, L., Edwards, K., and Malmsten, M. (2007) Effect of lipid headgroup composition on the interaction between melittin and lipid bilayers. *J. Colloid Interface Sci. 311*, 59–69.
6. Lee, M. T., Hung, W. C., Chen, F. Y., and Huang, H. W. (2008) Mechanism and kinetics of pore formation in membranes by water-soluble amphipathic peptides. *Proc. Natl. Acad. Sci. U.S.A. 105*, 5087–5092.
7. Klocek, G., and Seelig, J. (2008) Melittin interaction with sulfated cell surface sugars. *Biochemistry 47*, 2841–2849.
8. Vogel, H. (1981) Incorporation of melittin into phosphatidylcholine bilayers. Study of binding and conformational changes. *FEBS Lett. 134*, 37–42.
9. Batenburg, A. M., van Esch, J. H., and de Kruijff, B. (1988) Melittin-induced changes of the macroscopic structure of phosphatidylethanolamines. *Biochemistry 27*, 2324–2331.
10. Kuchinka, E., and Seelig, J. (1989) Interaction of melittin with phosphatidylcholine membranes. Binding isotherm and lipid headgroup conformation. *Biochemistry 28*, 4216–4221.
11. Schwarz, G., and Beschiaschvili, G. (1989) Thermodynamic and kinetic studies on the association of melittin with a phospholipid bilayer. *Biochim. Biophys. Acta 979*, 82–90.

12. Beschiaschvili, G., and Seelig, J. (1990) Melittin binding to mixed phosphatidylglycerol/phosphatidylcholine membranes. *Biochemistry 29*, 52–58.
13. Ladokhin, A. S., and White, S. H. (1999) Folding of amphipathic α-helices on membranes: Energetics of helix formation by melittin. *J. Mol. Biol. 285*, 1363–1369.
14. Quay, S. C., and Condie, C. C. (1983) Conformational studies of aqueous melittin: Thermodynamic parameters of the monomer-tetramer self-association reaction. *Biochemistry 22*, 695–700.
15. Wilcox, W., and Eisenberg, D. (1992) Thermodynamics of melittin tetramerization determined by circular dichroism and implications for protein folding. *Protein Sci. 1*, 641–653.
16. Goto, Y., and Hagihara, Y. (1992) Mechanism of the conformational transition of melittin. *Biochemistry 31*, 732–738.
17. Oren, Z., and Shai, Y. (1997) Selective lysis of bacteria but not mammalian cells by diastereomers of melittin: Structure-function study. *Biochemistry 36*, 1826–1835.
18. Reed, J., and Reed, T. A. (1997) A set of constructed type spectra for the practical estimation of peptide secondary structure from circular dichroism. *Anal. Biochem. 254*, 36–40.
19. Seelig, J., Nebel, S., Ganz, P., and Bruns, C. (1993) Electrostatic and nonpolar peptide-membrane interactions. Lipid binding and functional properties of somatostatin analogues of charge $z = +1$ to $z = +3$. *Biochemistry 32*, 9714–9721.
20. Aveyard, R., and Haydon, D. A. (1973) *An introduction to the principles of surface chemistry*, Cambridge University Press, London.
21. McLaughlin, S. A. (1977) Electrostatic potentials at membrane-solution interfaces. *Curr. Top. Membr. Transp. 9*, 71–144.
22. Eisenberg, M., Gresalfi, T., Riccio, T., and McLaughlin, S. (1979) Adsorption of monovalent cations to bilayer membranes containing negative phospholipids. *Biochemistry 18*, 5213–5223.
23. Rex, S., Bian, J., Silvius, J. R., and Lafleur, M. (2002) The presence of PEG-lipids in liposomes does not reduce melittin binding but decreases melittin-induced leakage. *Biochim. Biophys. Acta 1558*, 211–221.
24. Stanislawski, B., and Ruterjans, H. (1987) C-13-NMR Investigation of the Insertion of the Bee Venom Melittin into Lecithin Vesicles. *Eur. Biophys. J. Biophys. Lett. 15*, 1–12.
25. Batenburg, A. M., Hibbeln, J. C. L., and Dekruijff, B. (1987) Lipid Specific Penetration of Melittin into Phospholipid Model Membranes. *Biochim. Biophys. Acta 903*, 155–165.
26. Batenburg, A. M., Vanesch, J. H., Leunissenbijvelt, J., Verkleij, A. J., and Dekruijff, B. (1987) Interaction of Melittin with Negatively Charged Phospholipids: Consequences for Lipid Organization. *FEBS Lett. 223*, 148–154.
27. Altenbach, C., and Hubbell, W. L. (1988) The Aggregation State of Spin-Labeled Melittin in Solution and Bound to Phospholipid-Membranes: Evidence That Membrane-Bound Melittin Is Monomeric. *Proteins:. Struct., Funct., Genet. 3*, 230–242.
28. Matsuzaki, K., Yoneyama, S., and Miyajima, K. (1997) Pore formation and translocation of melittin. *Biophys. J. 73*, 831–838.
29. Wenk, M. R., and Seelig, J. (1998) Magainin 2 amide interaction with lipid membranes: Calorimetric detection of peptide binding and pore formation. *Biochemistry 37*, 3909–3916.
30. Wieprecht, T., Apostolov, O., Beyermann, M., and Seelig, J. (1999) Thermodynamics of the α helix-coil transition of amphipathic peptides in a membrane environment: Implications for the peptide-membrane binding equilibrium. *J. Mol. Biol. 294*, 785–794.
31. Wieprecht, T., Apostolov, O., Beyermann, M., and Seelig, J. (2000) Membrane binding and pore formation of the antibacterial peptide PGLa: Thermodynamic and mechanistic aspects. *Biochemistry 39*, 442–452.
32. Seelig, J. (1997) Titration calorimetry of lipid-peptide interactions. *Biochim. Biophys. Acta 1331*, 103–116.
33. Lichtenberg, D., Opatowski, E., and Kozlov, M. M. (2000) Phase boundaries in mixtures of membrane-forming amphiphiles and micelle-forming amphiphiles. *Biochim. Biophys. Acta 1508*, 1–19.
34. Lee, M. T., Chen, F. Y., and Huang, H. W. (2004) Energetics of pore formation induced by membrane active peptides. *Biochemistry 43*, 3590–3599.
35. Wieprecht, T., Apostolov, O., and Seelig, J. (2000) Binding of the antibacterial peptide magainin 2 amide to small and large unilamellar vesicles. *Biophys. Chem. 85*, 187–198.
36. Meier, M., and Seelig, J. (2007) Thermodynamics of the coil ↔ β-sheet transition in a membrane environment. *J. Mol. Biol. 369*, 277–289.
37. Meier, M., and Seelig, J. (2008) Length dependence of the coil ↔ β-sheet transition in a membrane environment. *J. Am. Chem. Soc. 130*, 1017–1024.
38. Baker, B. M., and Murphy, K. P. (1998) Prediction of binding energetics from structure using empirical parameterization. *Methods Enzymol. 295*, 294–315.
39. Richards, F. M. (1977) Areas, volumes, packing and protein structure. *Annu. Rev. Biophys. Bioeng. 6*, 151–176.
40. Heyn, M. P., and Bretz, R. (1975) The self-association of ATP: Thermodynamics and geometry. *Biophys. Chem. 3*, 35–45.
41. Robinson, B. H., Seelig, A., and Schwarz, G. (1975) in *Chemical and Biological Applications of Relaxation Spectrometry* (Wyn-Jones, H., Ed.) pp 481−485, Reidel, Dordrecht, The Netherlands.
42. Terzi, E., Holzemann, G., and Seelig, J. (1994) Reversible random coil-β-sheet transition of the Alzheimer β-amyloid fragment (25−35). *Biochemistry 33*, 1345–1350.
43. Nagle, J. F., and Tristram-Nagle, S. (2000) Structure of lipid bilayers. *Biochim. Biophys. Acta 1469*, 159–195.
44. Hirota, N., Mizuno, K., and Goto, Y. (1998) Group additive contributions to the alcohol-induced α helix formation of melittin: Implication for the mechanism of the alcohol effects on proteins. *J. Mol. Biol. 275*, 365–378.
45. Li, Y., Han, X., and Tamm, L. K. (2003) Thermodynamics of fusion peptide-membrane interactions. *Biochemistry 42*, 7245–7251.

BI802127H